Award Number: G13AP00028

Source Scaling Relations of Subduction Earthquakes for Strong Ground Motion and Tsunami Prediction

FINAL REPORT

January 7, 2015

Paul Somerville, Andreas Skarlatoudis and Hong Kie Thio*

URS Group, Inc.

915 Wilshire Boulevard
Los Angeles, CA 90017

Tel: (213) 996-2200
Fax: (213) 996-2290

*Email: paul.somerville@urs.com

Research supported by the U.S. Geological Survey (USGS), Department of the Interior, under award number G13AP00028. The views and conclusions contained in this document are those of the authors and should not be interpreted as necessarily representing the official policies, either expressed or implied, of the U.S. Government.

Table of Contents

Source Scaling Relations of Subduction Earthquakes for Strong Ground Motion and Tsunami Prediction

SUMMARY

The recording on high-resolution, broadband seismic networks of several great interface subduction earthquakes during the last decade provides an excellent opportunity to extend source scaling relations to very large magnitudes and to place constraints on the potential range of source parameters for these events. At present, there is a wide range of uncertainty in the median rupture areas predicted for a given seismic moment by current relationships between magnitude and rupture area for subduction earthquakes. Our goal is to develop an updated set of earthquake source scaling relations that will reduce this current large degree of epistemic uncertainty and improve the accuracy of seismic hazard analysis and the prediction of the strong motion characteristics and tsunamis of future subduction earthquakes. In order to achieve this goal we compiled a database of slip models of interface earthquakes that occurred worldwide with moment magnitudes ranging from **M** 6.75 to **M** 9.1.

We characterized the seismic sources based on well-established criteria to estimate the asperity areas and the average slip on the faults and we used these parameters to compute an updated set of magnitude scaling relations of the various characteristics of the fault. Additionally, we followed an alternative approach to quantifying slip models for use in developing characteristic slip models of future earthquakes. This involved analyzing the 2-D Fourier transforms of the slip functions of the compiled database and deriving a wavenumber spectral model of the slip distribution.

INTRODUCTION

The ability to predict the ground motions and tsunamis from great subduction earthquakes requires reliable source scaling relations for subduction earthquakes. At present, there is a range of over a factor of 3 in the median rupture areas predicted for a given magnitude by current relationships between magnitude and rupture area for subduction earthquakes. For a given rupture area, there is a range of over 0.5 magnitude unit and a factor of over 5 in seismic moment in the median size of the predicted great earthquakes. This study aims to reduce this large epistemic uncertainty in the median values of the scaling relations.

After a long period of quiescence following the 1964 **M** 9.1 Alaska earthquake, several great subduction earthquakes have occurred during the last decade, including the 2001 **M** 8.4 Arequipa, Peru, 2004 **M** 9.1 Sumatra, 2010 **M** 8.8 Chile, and 2011 **M** 9.0 Tohoku earthquakes. The recording of these events on modern digital seismic networks provides an important opportunity to extend the source scaling relations of subduction earthquakes to very large magnitudes, and to place constraints on the potential range of source parameters for these events. Moreover, information about the source characteristics of these recent earthquakes is much more reliable and useful than that of older large

earthquakes. This information includes the spatial distribution of slip and slip velocity on the fault, which is derived from strong motion recordings and in turn is required for the simulation of strong ground motions and tsunamis. Geodetic and tsunami data are also useful for providing constraints on the spatial distribution of slip on the fault.

For predicting strong ground motions, we need to characterize the earthquake source in the frequency band of about 0.1 to 10 Hz or above and for tsunamis we need to characterize the earthquake source in the frequency band of 0 to 0.01 Hz. Our goal therefore is to develop earthquake source scaling relations for subduction earthquakes over the very broad frequency range of 0 to 10 Hz or above, so that they can be applied to the prediction of both strong ground motions and tsunamis. We distinguish two categories of kinematic source parameters. The first category, consisting of "outer" parameters, includes relationships between seismic moment and rupture length, rupture width, rupture area, and average displacement. These parameters are needed for predicting both ground motions and tsunamis. The second category, consisting of "inner" parameters that describe the heterogeneities of slip and slip velocity (asperities) on the fault rupture surface, includes relations between seismic moment and the spatial and temporal distribution of slip and slip velocity on the fault. The temporal inner parameters are of most importance for the prediction of strong ground motions, which are highly dependent on slip velocity and rupture velocity, but the spatial distribution of slip is also important for tsunami simulation. In the present study we analyze the scaling with seismic moment (M_o) of rupture width (W), rupture area (S), average slip (D) and maximum slip (D_a) for the "outer" parameters and total asperity area (S_a) for the "inner" parameters.

Following an alternative approach, we use the spatial wavenumber spectrum as an additional method of describing the heterogeneity of slip on the fault surface. We analyze the 2-D Fourier transforms of the slip functions of our database with the two dimensions being the dimension along-strike and the dimension down-dip. The Fourier transform describes the relative amplitudes of the different spatial wavelengths in the slip model. We assume that the wavenumber spectra in the along-strike and down-dip directions to have a self-similar scaling with moment magnitude **M** and by performing a least squares fit to these data we derive a wavenumber spectral model of the slip distribution for use in characterizing future earthquakes.

COMPILATION OF EARTHQUAKE RUPTURE MODEL DATABASE

We compiled an updated database of interface earthquakes that occurred worldwide in the major subduction zones, with moment magnitudes ranging from **M** 6.75 to **M** 9.1. Information regarding the earthquake location and magnitude, the sources used for the compilation of the database, as well the adopted values of the basic source parameters used in the analysis can be found in Table 1.

Table 1. Earthquakes used for source characterization in present study.

	Region	Date	Seismic Moment (Nm)	Mw	S (km^2)	S_a (km^2)	D (m)	D_a (m)	W (km)	References
1	Hyuga-nada, Japan	2-Dec-96	1.50E+19	6.72	179	154	0.42	0.92	-	Yagi et al. (1999)
2	Peru	9-Nov-74	5.40E+19	7.09	3000	600	0.54	1.16	50	Somerville et al. (2002)
3	Playa Azul	25-Oct-81	7.14E+19	7.17	2700	400	0.74	2.37	60	Somerville et al. (2002)
4	Zihuatanejo	21-Sep-85	1.35E+20	7.35	3150	1350	1.02	1.54	60	Somerville et al. (2002)
5	Near Coast Of Guerrero, Mexico	3-Mar-12	1.41E+20	7.37	4125	1050	0.41	0.20	100	Wei (Caltech, Oaxaca 2012)
6	Honshu, Japan	16-Aug-05	2.00E+20	7.47	3584	960	0.15	0.70	72	Shao and Ji (UCSB, Honshu 2005)
7	Colima, Mexico	22-Jan-03	2.30E+20	7.51	5950	1350	0.61	1.30	85	Yagi et al. (2004)
8	Hyuga-nada, Japan	1-Apr-68	2.50E+20	7.53	1377	1053	1.32	2.90	-	Yagi et al. (1998)
9	Costa Rica	5-Sep-12	2.54E+20	7.54	18000	3520	0.29	0.95	120	Hayes (NEIC, Costa Rica 2012)
10	East of Sulangan, Philippines	31-Aug-12	2.72E+20	7.56	4608	1440	0.42	1.90	90	Hayes (USGS, Philippines 2012)
11	Papua	3-Jan-09	2.82E+20	7.57	11520	1680	0.59	2.00	96	Hayes (NEIC, Papua 2009)
12	Vanuatu	7-Oct-09	2.82E+20	7.57	4200	1680	0.87	2.05	60	Sladen (Caltech, Vanuatu 2009)
13	Fiordland, New Zealand	15-Jul-09	2.82E+20	7.57	10752	2560	0.63	2.60	96	Hayes (NEIC, New Zealand 2009)
14	Nihonkai-chubu, Japan	26-May-83	3.00E+20	7.58	2700	-	3.17	-	-	Fukuyama and Irikura (1986)
15	Hokkaido- Nansei	12-Nov-93	3.40E+20	7.62	14000	2300	0.64	1.64	70	Mendoza and Fukuyama (1996)
16	Tocopilla, Chile	14-Nov-07	3.98E+20	7.67	18954	7695	0.88	1.75	126	Sladen (Caltech, Tocopilla 2007)
17	Sanrikuki, Japan	28-Dec-94	3.99E+20	7.67	15400	2600	0.71	1.95	140	Nagai et al. (2001)
18	Masset,Canada	28-Oct-12	4.27E+20	7.69	4800	1440	1.57	4.80	60	Shao and Ji (UCSB, Masset 2012)
19	Sanriku-haruka-oki, Japan	28-Dec-94	4.40E+20	7.70	2800	2800	0.71	1.93	-	Nagai et al. (2001)
20	Kanto , Japan	1-Sep-23	7.60E+20	7.85	2340	2210	2.54	5.60	-	Wald and Somerville (1995)
21	Pagai, Indonesia	12-Sep-07	7.94E+20	7.87	21875	6500	0.55	1.47	90	Ji and Zeng (Pagai 2007)
22	Colima, Mexico	9-Oct-95	9.67E+20	7.92	17000	2800	1.18	2.80	100	Mendoza and Hartzell (1999)
23	Pisco, Peru	15-Aug-07	1.12E+21	7.97	20736	5508	1.63	3.80	108	Ji and Zeng (Peru 2007)
24	Samoa	29-Sep-09	1.12E+21	7.97	7243	1983	3.33	8.98	49	Hayes (NEIC, Samoa 2009)
25	Michoacan, Mexico	19-Sep-85	1.15E+21	7.97	25020	5004	1.40	2.95	139	Mendoza and Hartzell (1989)

26	Peru	3-Oct-74	1.20E+21	7.99	28000	6066	1.30	2.19	112	Somerville et al. (2002)
27	Nazca Ridge, Peru	12-Nov-96	1.38E+21	8.03	36000	9072	0.77	1.53	120	Spence et al. (1999)
28	Solomon Islands	1-Apr-07	1.58E+21	8.07	21600	6600	1.47	2.70	80	Ji (UCSB, Solomon Islands 2007)
29	Tokachi-oki, Japan	25-Sep-03	1.92E+21	8.12	22100	5600	1.46	3.15	170	Yagi (2004)
30	Central Chile	3-Mar-85	1.96E+21	8.13	34425	9675	1.92	1.75	165	Mendoza et al. (1994)
31	Tonankai, Japan	7-Dec-44	2.40E+21	8.19	4000	4800	1.05	1.78	-	Ichinose et al.(2003)
32	Kuril Islands	15-Nov-06	3.16E+21	8.27	35750	10000	1.69	5.10	138	Ji (UCSB, Kuril 2006)
33	Tokachi-oki, Japan	16-May-68	3.50E+21	8.30	6800	5600	2.31	5.49	-	Nagai et al.(2001)
34	Arequipa	23-Jun-01	3.70E+21	8.31	80000	20800	1.22	2.48	200	Somerville et al. (2003)
35	Nankai, Japan	21-Dec-46	3.90E+21	8.33	52650	-	1.98	-	-	Tanioka and Satake (2001a)
36	Benkulu, Indonesia	12-Sep-07	4.47E+21	8.37	73140	28331	0.90	1.85	160	Ji (UCSB, Benkulu 2007)
37	Sumatra	28-Mar-05	1.17E+22	8.65	86400	27200	2.56	5.45	260	Shao and Ji (UCSB, Sumatra 2005)
38	Aleutian	9-Mar-57	1.20E+22	8.65	93750	30000	3.10	-	-	Johnson et al. (1994)
39	Kamchatka	4-Nov-52	1.50E+22	8.72	70000	20000	5.50	-	-	Johnson and Satake, (1999)
40	Maule, Chile	27-Feb-10	1.55E+22	8.73	115000	31875	4.13	9.00	200	Lorito et al. (2011)
41	Tohoku-Oki, Japan	11-Mar-11	4.20E+22	9.02	81000	18900	10.51	22.97	180	Yokota et al., (2011)
42	Alaska	27-Mar-64	5.52E+22	9.09	225000	30000	4.00	11.30	265.6	Ichinose et al., (2007)
43	Sumatra, Indonesia	26-Dec-04	6.50E+22	9.14	265237	27571	3.90	6.70	193	Ammon et al. (2005)
44	Chile	22-May-60	7.20E+22	9.17	135000	40000	10.60	-	-	Fujii and Satake (2013)

The locations of these earthquakes are shown in the map of Figure 1. The majority of the finite-fault rupture models of the earthquakes in Table 1 were available from the online database "Finite Source Rupture Model Database" (http://equake-rc.info/SRCMOD/). Other major sources used for collecting slip models and information about them were Murotani et al. (2008; 2013) and Somerville et al. (2002). To characterize asperities in these cases we use the definition given in Somerville et al. (1999): *an asperity is initially defined to enclose fault elements whose slip is 1.5 or more times larger than the average slip over the fault and is subdivided if any row or column has an average slip less than 1.5 times the average slip.*

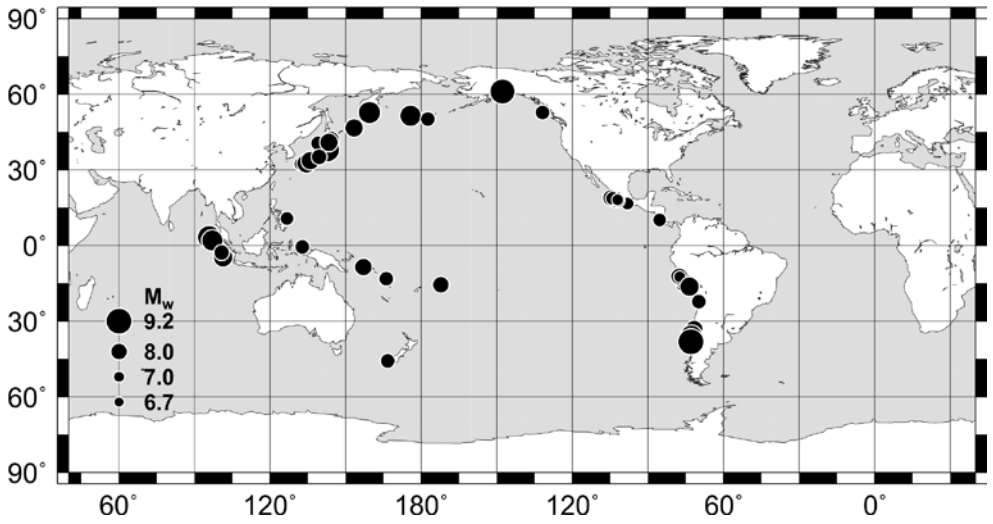

Figure 1. Map showing the locations of the earthquakes listed in Table 1.

When the original slip model was not available in the database we used the source characterization parameters reported in the literature. We evaluated all available rupture models of each earthquake in order to understand the uncertainty in the slip model inversion process and to identify the best constrained features of the rupture models of these earthquakes. When an earthquake had more than one available rupture model we selected the one that was based on the largest number of strong motion or teleseismic data for use in our analysis. As an example, multiple rupture models of the Maule, Chile earthquake are listed in Table 2. Following the aforementioned procedure, we chose the model proposed by Lorito et al. (2011). Comparison of the published models reveals that a large variability exists for all of the parameters. As seen in Table 2, the variability for specific models and parameters can be up to 50%, which indicates that judgment should be exercised in selecting the slip model that is most appropriate for a specific application.

Table 2. Published rupture models for the Maule, Chile earthquake (#40 in Table 1) reviewed in the present study. The Lorito et al. (2011) rupture model was the preferred one. The absolute percentage difference of each parameter with respect to that of the preferred model is denoted in parentheses.

Seismic moment (Nm)	Length (km)	Width (km)	Rupture Area (km2)	Trimmed Rupture Area (km2)	Asperity Rupture Area (km2)	Average Slip (m)	Asperity Slip (m)	Author
1.74E+22	570	180	102600.0	102600.0 (10.8%)	23850.0 (25.2%)	2.29 (44.6%)	4.15 (53.9%)	Sladen (Caltech, Maule 2010)
1.60E+22	540	200	108000.0	86400.0 (24.9%)	26400.0 (17.2%)	3.87 (6.3%)	9.25 (2.8%)	Hayes (NEIC, Maule 2010)
1.78E+22	680	256.1	174148.0	74436.9 (35.3%)	18904.6 (40.7%)	2.69 (34.9%)	10.20 (13.3%)	Luttrell et al. (2011)
2.51E+22	600	187	112200.0	84150.0 (26.8%)	18360.0 (42.4%)	4.05 (1.9%)	8.80 (2.2%)	Shao et al. (UCSB, Maule 2010)
1.55E+22	**650**	**200**	**130000.0**	**115000.0**	**31875.0**	**4.13**	**9.00**	**Lorito et al. (2011)**

DEVELOPMENT OF SOURCE SCALING RELATIONSHIPS

Self-similar models

We used the updated database of finite-fault rupture models that we compiled to produce scaling relations of the various source parameters. In order for the relations to be self-consistent, for the rupture area (S), total asperity area (S_a) and average slip (D) we used only finite-fault rupture models for which all three quantities were available. For maximum slip (D_{max}) and width (W) we used all available data. For the regressions we applied the Levenberg-Marquardt algorithm (Levenberg, 1944; Marquardt D., 1963) through the least-squares method. We initially fit the data using self-similar relationships with a constrained slope. The logarithms of S and S_a (km^2) are proportional to two-thirds of seismic moment, while the logarithms of D and D_{max} (m) are proportional to one-third of seismic moment:

$$\log(D) = \log(c_1) + \frac{1}{3}\log(M_0)\ ,\ \log(S) = \log(c_2) + \frac{2}{3}\log(M_0) \qquad (1)$$

where c_1 and c_2 are the regression coefficients and M_0 is seismic moment. We used base 10 logarithms in the regressions. The coefficients and the standard deviations derived are given in Table 3.

Table 3. Self-similar scaling relations, regression coefficients and standard deviations

	Mo-S		*Mo-D*		*Mo-S_a*		*S-S_a*		*Mo-D_{max}*	
	c_1	***σ***	***c_2***	***σ***	***c_1***	***σ***	***c***	***σ***	***c_2***	***σ***
Present Study	**1.77E-10**	**1.498**	**1.23E-07**	**1.527**	**4.16E-11**	**1.613**	**0.24**	**1.40**	**5.00E-07**	**1.508**
Murotani et al. (2013)	1.34E-10	1.540	1.66E-07	1.640	2.81E-11	1.720	0.20	1.41	-	-
Murotani et al. (2008)	1.48E-10	1.610	1.48E-07	1.720	2.89E-11	1.780	0.20	1.41	-	-
Somerville et al. (2002)	2.41E-10	-	1.14E-07	-	5.62E-11	-	0.25	-		

In Figure 2 the derived relations for S and S_a (black solid lines) are plotted together with the data used in the analysis (different symbols to account for the various data sources, Sea2014 - Present study; Sea2002 - Somerville et al., 2002; Mea2013 - Murotani et al., 2013; Mea2008 - Murotani et al., 2008). The shaded area represents the ± 1 standard deviation. Similarly, the derived relations for D and D_{max} are shown in Figure 3.

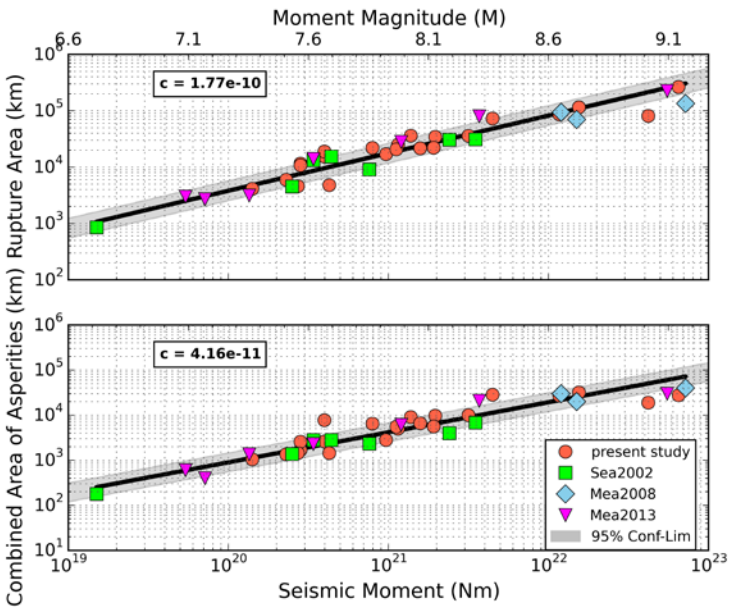

Figure 2. Scaling of the rupture area and the combined area of asperities area with seismic moment, plotted together with data from various studies:[Sea2002 - Somerville et al., 2002; Mea2013 - Murotani et al., 2013; Mea2008 - Murotani et al., 2008]. The shaded area indicates the ±1 standard deviation limits.

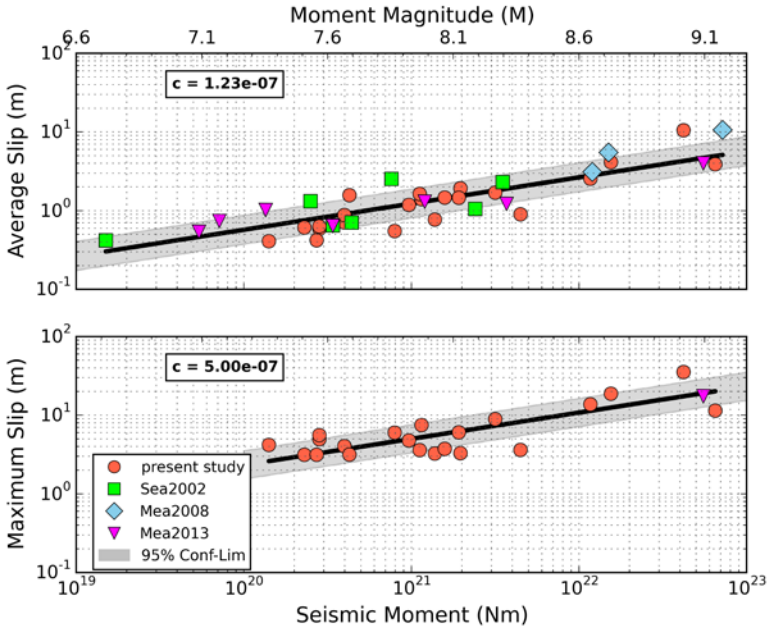

Figure 3. Scaling of average and maximum slip with seismic moment, plotted together with data from various studies; colors and symbols are the same as in the previous figure. The shaded area indicates the ±1 standard deviation limits.

In Figure 4 the scaling between the combined area of asperities and rupture area is shown. The combined area of asperities is found to be 0.24 times the rupture area, close to the results of Somerville et al. (2002).

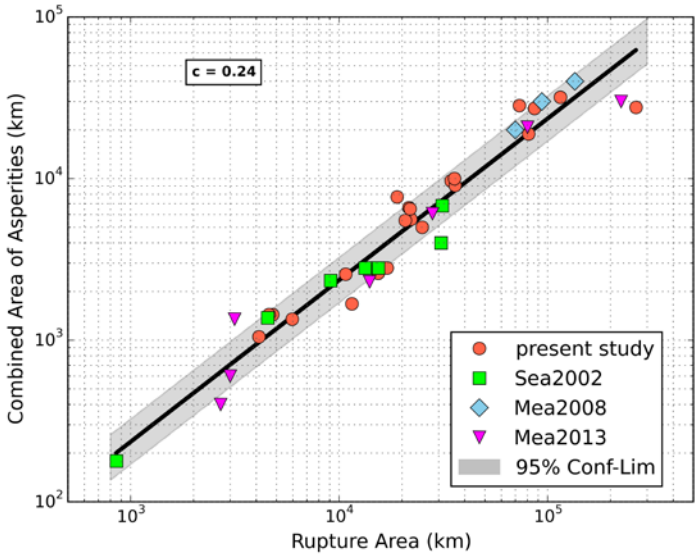

Figure 4. Relationship between combined area of asperities and rupture area; colors and symbols are the same as in the previous figure.

The shaded area indicates the ±1 standard deviation limits. The residual analysis (data – predicted plotted against M_0) presented in Figure 5 is used to examine the regression quality and identify potential trends in the dataset. For all parameters studied the residuals do not exhibit any significant trends, although the residuals are all zero or negative for rupture area and combined area of asperities for magnitudes of 9 and larger.

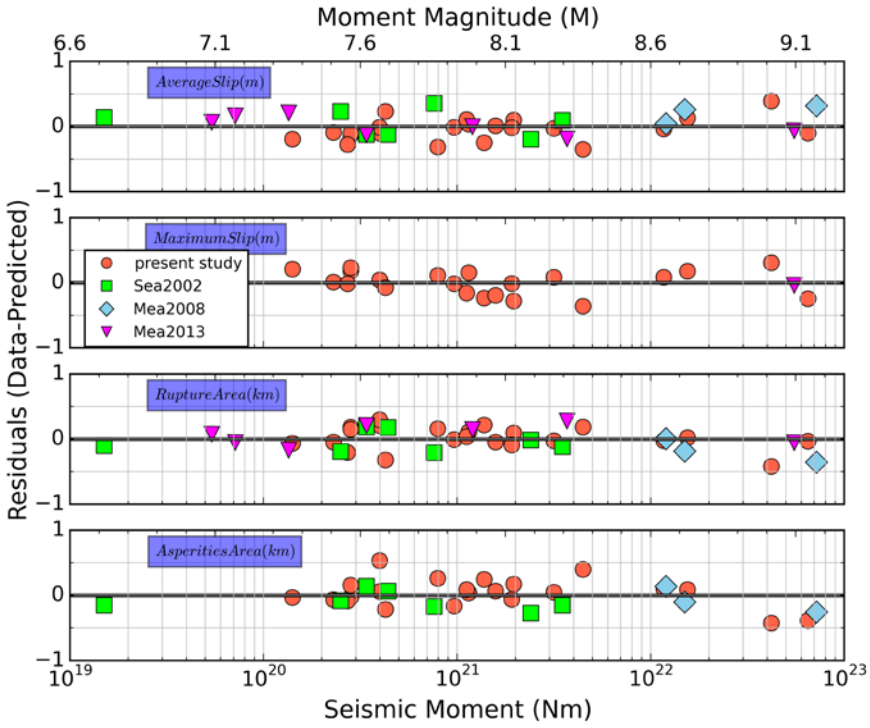

Figure 5. Residual (data-predicted) plots against seismic moment for average and maximum slip, rupture area and total area of asperities. Colors and symbols are the same as in the previous figure.

Non self-similar models

We assumed self-similar scaling laws in performing the regression analysis in the previous section. However, there are studies (e.g. Tajima et al., 2013; Strasser et al., 2010; Papazachos et al., 2004) that suggest a departure from self-similarity of the rupture area and slip of the fault. We relaxed the constraint of self-similarity and fit the data to a non-self-similar relationship of the form:

$$\log(Y) = \log(c_a) + c_b \log(M_0) \qquad (2)$$

where Y corresponds to the different source parameters and c_a, c_b are the regression coefficients. The coefficient values along with the standard deviations from the regressions are listed in Table 4.

Table 4. Non self-similar scaling relations, regression coefficients and standard deviations.

Source Parameter	c_a	c_b	σ
Rupture Area (A)	1.72E-09	4.17	1.481
Total Asperity Area (A_a)	4.81E-10	4.13	1.596
Average Slip (D)	3.39E-08	2.29	1.522
Maximum Slip (D_{max})	2.70E-06	1.99	1.501
Width (W_1)	6.75E-03	1.59	1.264
Width (W_2)	1.66E-04	1.90	1.259

In Figures 6 through 8 the regression results for the non-self-similar functional forms are shown with the dark red lines.

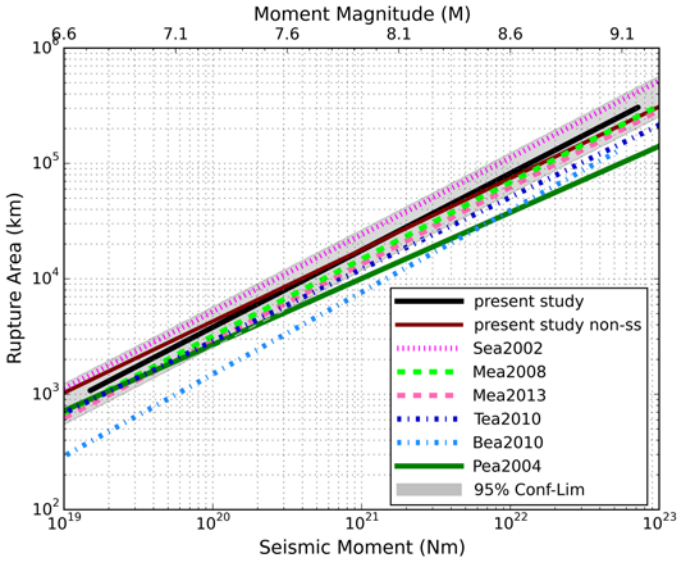

Figure 6. Scaling relations of the rupture area from various studies with respect to seismic moment [Sea2002 - Somerville et al., 2002; Mea2013 - Murotani et al., 2013; Mea2008 - Murotani et al., 2008; Tea2010 – Strasser et al., 2010; Bea2010 – Blaser et al., 2010; Pea2004 – Papazachos et al., 2004]. The shaded area indicates the ±1 standard deviation limits of this study's self-similar model.

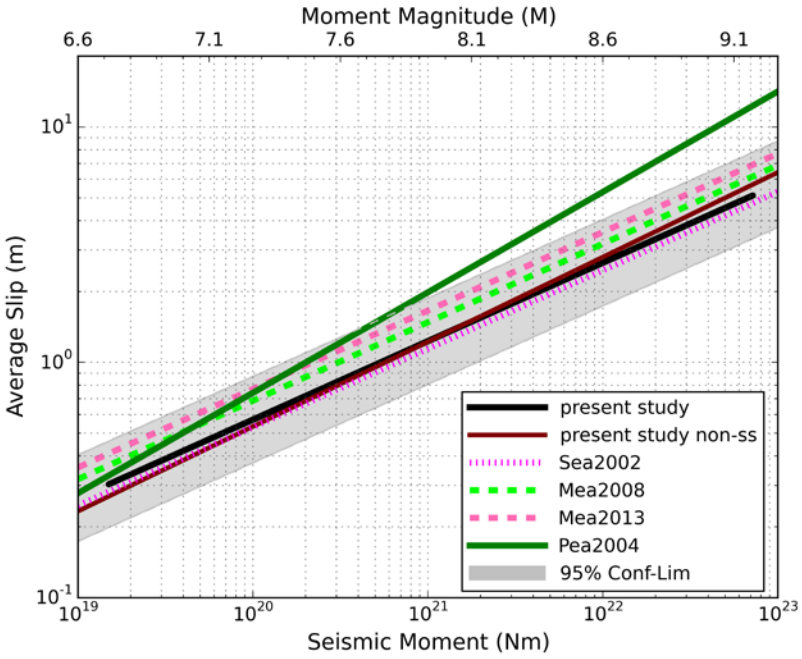

Figure 7. Scaling relations of the average slip from various studies with respect to seismic moment. Colors and line styles are the same as in the previous figure. The shaded area indicates the ±1 standard deviation limits of this study's self-similar model.

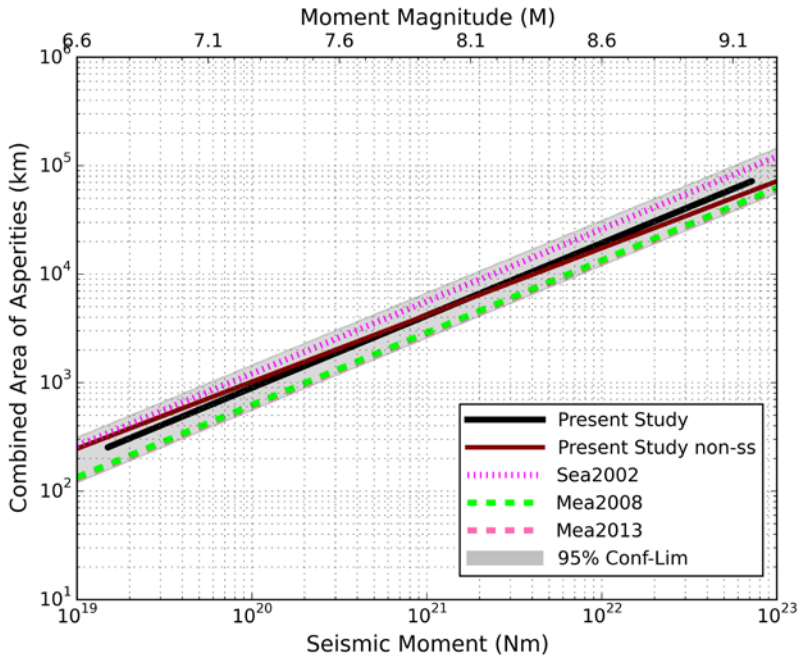

Figure 8. Scaling relations of the total area of asperities from various studies with respect to seismic moment. Colors and line styles are the same as in the previous figure. The shaded area indicates the ±1 standard deviation limits of this study's self-similar model.

Comparison with the results from the self-similar functional forms (black curves) does not exhibit substantial differences for the average slip and rupture areas. The differences in data fit between the unconstrained models and those that are constrained to be self-similar are not large and are not statistically significant, as shown from the low t-test values computed for the slopes of rupture and asperity area and average slip relations, -7.3E-10, -1.94E-10 and 4.13E-08, respectively. Therefore, we prefer to retain the simplicity of using the self-similar relations as found in some of the previous studies (Murotani et al., 2013; 2008, Somerville et al., 2002).

Fault width scaling models

In Figure 9 the scaling of fault width with respect to seismic moment is presented. The scaling coefficients from the least squares fit are shown in Table 4 (model W_1). Both data (Figure 9) and the residual distribution (Figure 10, solid symbols) justify the linear model up to the maximum magnitude that was used in the regression (**M**=9.17 for Sumatra 2004 earthquake). However there are studies (e.g. Tajima et al., 2013, Blaser et al., 2010) that indicate that beyond a certain magnitude the fault width tends to a constant value (saturates). We tested this assumption by fitting a bi-linear model that saturates for magnitudes **M**>8.4, consistent with the model of Tajima et al. (2013). The regression coefficients for the bi-linear model are listed in Table 4 as model W_2 and the fit is depicted with the dashed line in Figure 9.

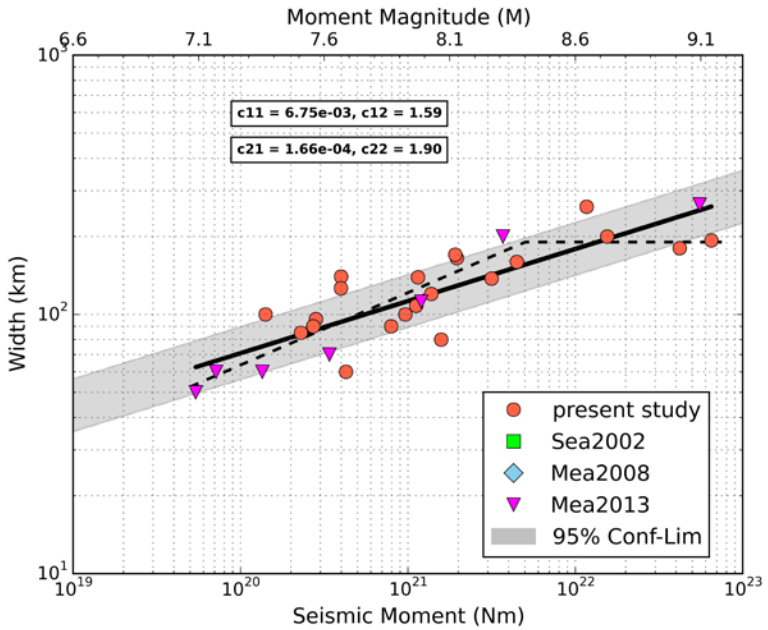

Figure 9. Scaling relation of fault width with respect to seismic moment. Colors and symbols are the same as in Figure 2. The dashed line corresponds to the bi-linear model used in the regressions (model #2 in figure legend). The shaded area indicates the ±1 standard deviation limits of the linear model.

The standard deviation of the bi-linear fit is slightly smaller than that for the linear fit, basically because the bi-linear model gives a better fit to the three data points at magnitudes **M**>9 (Alaska 1964, Sumatra 2004 and Tohoku 2011 earthquakes). In Figure 10 the open symbols represent the residuals from the bi-linear fit and it can be seen that the largest difference is observed only for these three points. We believe that this might be an indication of fault width saturation. The study of Tajima et al. (2013) also suggests saturation at a median width of 200 km, similar to our result in Figure 9. The limited number of data for **M**>8.3 and the poor constraint of the fit for **M**>9.0 do not provide definitive resolution of width saturation. However, we consider that width saturation at a median width of 200 km is most likely present, but may vary from one subduction zone to another.

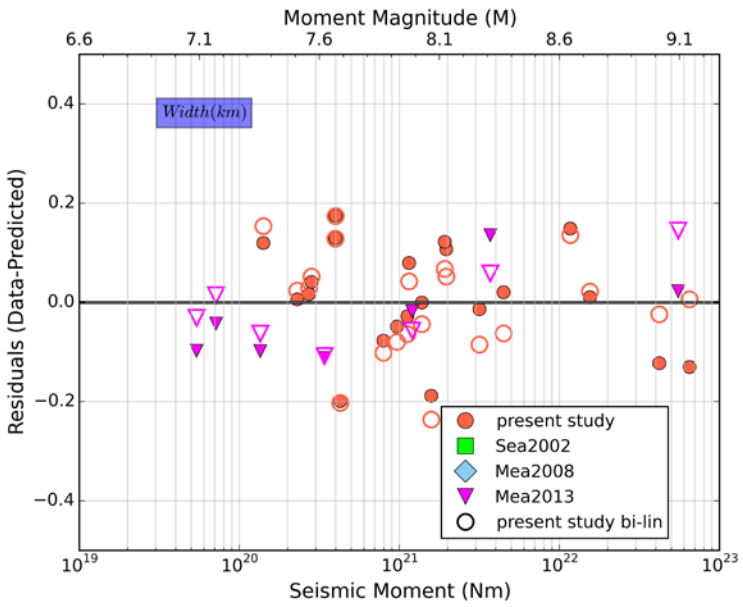

Figure 10. Residual (data-predicted) plots against seismic moment for average and maximum slip, rupture area and total asperities area. Colors and symbols are the same as in Figure 2. The open symbols denote the residuals for the bi-linear model used in the regressions.

CHARACTERIZATION BASED ON CORNER WAVENUMBERS

So far, we have made quantitative estimates of the parameters of slip models and analyzed their scaling with seismic moment. In this section, we follow an alternative approach to quantifying slip models for use in developing characteristic slip models of future earthquakes. This approach was originally described in Somerville et al. (1999) for crustal earthquakes but in the present study we apply the same model to subduction earthquakes.

The first step is to compute the 2D Fourier transforms of the slip functions summarized above with the two dimensions being the dimension along-strike and the dimension down-dip. The Fourier transform describes the relative amplitudes of the different spatial wavelengths (wavenumbers) in the slip model. Small wavenumbers are equivalent to long wavelengths and represent broad fluctuations of slip over the fault surface, while large wavenumbers are equivalent to short wavelengths and represent local fluctuations over the fault surface. The spatial sampling of the fault in the along-strike and down-dip directions controls the highest wavenumber (Nyquist wavenumber) for which the slip model is complete. The corner spatial wavenumbers were used to construct a wavenumber spectral model.

The slip models were resampled at 1 km spacing using 1st degree bivariate splines and they were padded with zeros to 1024 km in each direction to produce even sampling of the wavenumber spectra. We obtained the parameters of a wavenumber spectral model of the slip distribution in earthquakes by fitting a simple functional form to the wavenumber spectra of individual earthquakes. We used a 2D

Butterworth filter function to model the wavenumber amplitude spectrum which is described in the following relation:

$$amp(kx, ky) = \frac{1}{\sqrt{1+\left(\left(\frac{kx}{KCx}\right)^2+\left(\frac{ky}{KCy}\right)^2\right)^2}} \quad (3)$$

where $amp(kx, ky)$ is the 2D Fourier transform amplitudes, k_x and k_y are the wavenumbers and Kc_x and Kc_y are the corner wavenumbers, in each dimension. We fit relation (3) by using the damped least squares method in order to solve this non-linear problem. We performed 1000 iterations and the damping coefficient that was used had the value of λ=2E+11. An example of the procedure is shown in Figure 11 for two slip models [Kanto, Japan (1923) and Sumatra (2004)]. The estimated maximum spatial wavenumbers are listed in Table 5.

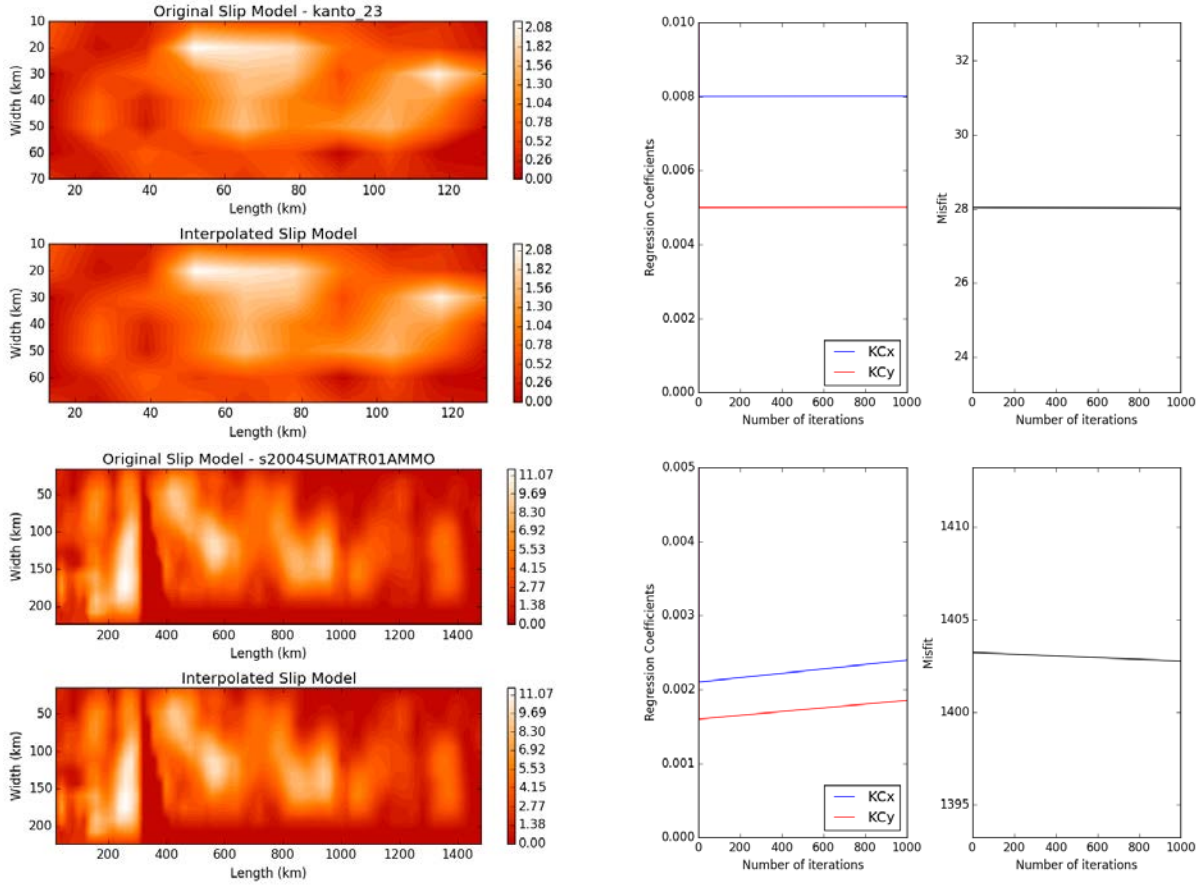

Figure 11. Left panel) Examples of original and interpolated slip models [upper plot: Kanto, Japan (1923) and bottom plot: Sumatra (2004)]. Right panel) Spectral decay fits for along strike and down dip directions.

In order to verify that the corner wavenumbers estimated from the regressions actually describe the decay of the amplitudes with wavenumber in each direction, we plotted the logarithm of the normalized amplitudes and compared them with the simplified model

$$\mathrm{amp(k)} = [1 + (\mathrm{k/Kc})^4]^{-\frac{1}{2}}, \qquad (4)$$

where Kc is the maximum wavenumber in each direction. For the two slip models in Figure 11, the fits are shown in Figure 12. The vertical lines depict the Nyquist wavenumbers of the original slip models, before resampling and padding, along x and y directions.

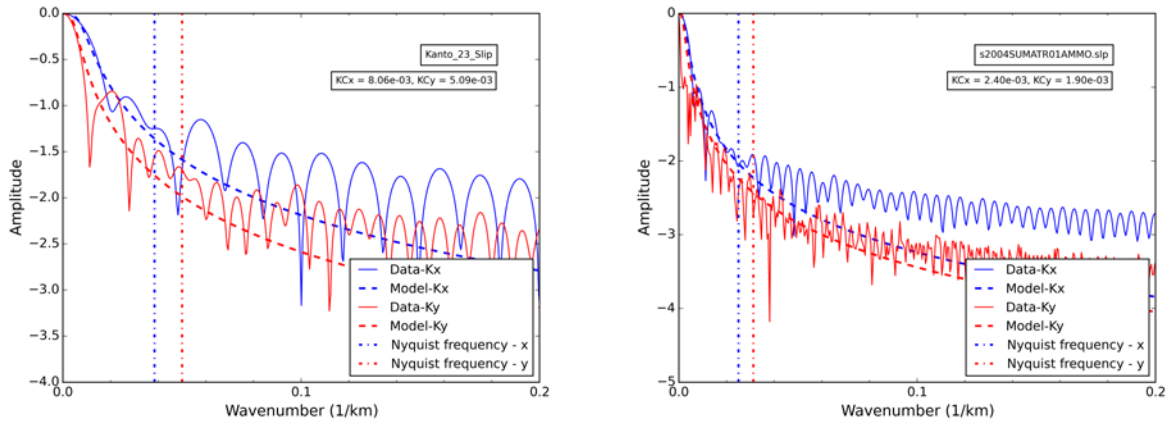

Figure 12. Spectral decay fits for along strike and down dip directions for Kanto, Japan (1923) and Sumatra (2004) slip models. The vertical lines depict the Nyquist wavenumber of the original slip models, before resampling and padding, along the x and y directions.

Table 5. Corner spatial wavenumbers of the slip models.

#	Slip Model	Date	Seismic Moment (Nm)	Magnitude (M)	KC_x (km^{-1})	KC_y (km^{-1})
1	Playa Azul	25-Oct-81	7.14E+19	7.17	0.010560	0.010310
2	Zihuatanejo	21-Sep-85	1.35E+20	7.35	0.005160	0.005100
3	Near Coast Of Guerrero, Mexico	3-Mar-12	1.41E+20	7.37	0.010690	0.010430
4	Colima, Mexico	22-Jan-03	2.30E+20	7.51	0.011000	0.010400
5	Costa Rica	5-Sep-12	2.54E+20	7.54	0.007085	0.005098
6	East of Sulangan, Philippines	31-Aug-12	2.72E+20	7.56	0.006147	0.005599
7	Fiordland, New Zealand	15-Jul-09	2.82E+20	7.57	0.008290	0.006740
8	Papua	3-Jan-09	2.82E+20	7.57	0.008140	0.006630
9	Vanuatu	7-Oct-09	2.82E+20	7.57	0.010070	0.006136
10	Hokkaido- Nansei	12-Nov-93	3.40E+20	7.62	0.008071	0.004121
11	Tocopilla, Chile	14-Nov-07	3.98E+20	7.67	0.005000	0.002400
12	Sanrikuki, Japan	28-Dec-94	3.99E+20	7.67	0.007000	0.003261
13	Masset,Canada	28-Oct-12	4.27E+20	7.69	0.015029	0.004176
14	Kanto , Japan	1-Sep-23	7.60E+20	7.85	0.008057	0.005088
15	Pagai, Indonesia	12-Sep-07	7.94E+20	7.87	0.006500	0.004000
16	Colima, Mexico	9-Oct-95	9.67E+20	7.92	0.007164	0.003320
17	Pisco, Peru	15-Aug-07	1.12E+21	7.97	0.006670	0.005190
18	Samoa	29-Sep-09	1.12E+21	7.97	0.010369	0.005690
19	Michoacan, Mexico	19-Sep-85	1.15E+21	7.97	0.004800	0.003900
20	Nazca Ridge, Peru	12-Nov-96	1.38E+21	8.03	0.004300	0.003300
21	Solomon Islands	1-Apr-07	1.58E+21	8.07	0.007139	0.003383
22	Tokachi-oki, Japan	25-Sep-03	1.92E+21	8.12	0.004694	0.004377
23	Central Chile	3-Mar-85	1.96E+21	8.13	0.004100	0.003300
24	Tonankai, Japan	7-Dec-44	2.40E+21	8.19	0.003300	0.002800

25	Kuril Islands	15-Nov-06	3.16E+21	8.27	0.005216	0.001898
26	Arequipa	23-Jun-01	3.70E+21	8.31	0.002770	0.001860
27	Benkulu, Indonesia	12-Sep-07	4.47E+21	8.37	0.003772	0.002229
28	Sumatra	28-Mar-05	1.17E+22	8.65	0.002895	0.002280
29	Maule, Chile	27-Feb-10	1.55E+22	8.73	0.003232	0.002274
30	Tohoku-Oki, Japan	11-Mar-11	4.20E+22	9.02	0.002402	0.003285
31	Alaska	27-Mar-64	5.52E+22	9.09	0.003010	0.002441
32	Sumatra, Indonesia	26-Dec-04	6.50E+22	9.14	0.002401	0.001900

The corner wavenumbers KC_x and KC_y in the along-strike and down-dip directions, respectively, were assumed each to have self-similar scaling with moment magnitude **M**. For self-similar scaling the logarithm of the corner wavenumber is proportional to one half the moment magnitude:

$$\log(KC_x) = c_x - 0.5\boldsymbol{M} \qquad (4)$$
$$\log(KC_y) = c_y - 0.5\boldsymbol{M}$$

The coefficients from the least squares fit are shown in Table 6. In Figure 13 the logarithms of the corner wavenumbers (c_x – top panel, c_y – bottom panel) are plotted together with the least squares fit. The shaded area corresponds to the ± 1 standard deviation. Based on the constant width model that we presented in the previous section, we additionally studied possible trends in c_y with fault width. The colored symbols in the lower panel of Figure 13 correspond to different fault width bins. The residual (data-predictions) distribution against **M** is shown in Figure 14. The residual plots verify that for the along strike dimension there is no apparent trend in our model. Similarly for c_y (down-dip direction) there is no dependence on fault width except for the largest three earthquakes with width greater than 160 km, consistent with the saturation of width shown in Figure 9.

Table 6. Scaling coefficients of the corner wavenumbers.

c_x	σ	c_y	σ
1.75	0.146	1.59	0.168

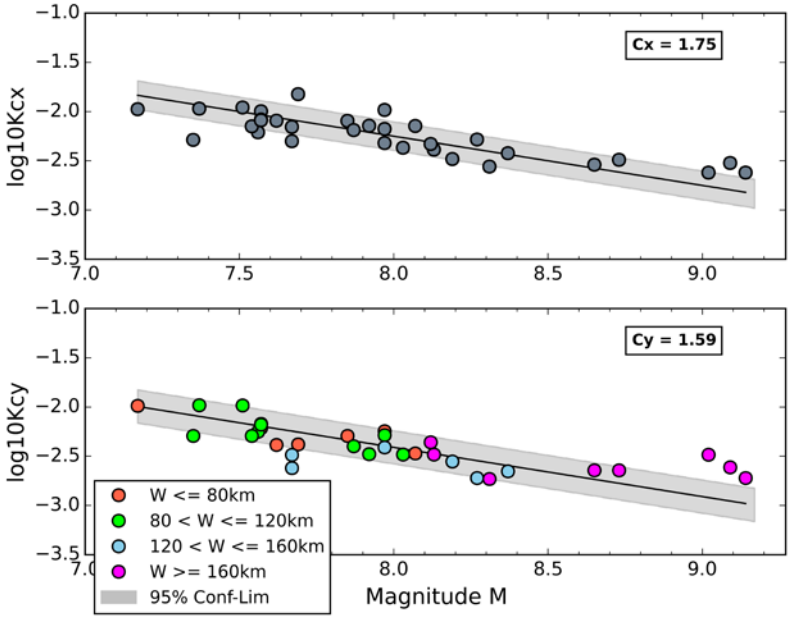

Figure 13. Least square fits of equations (4). The shaded area indicates the ±1 standard deviation limits. The colored symbols in the bottom panel correspond to different fault width bins.

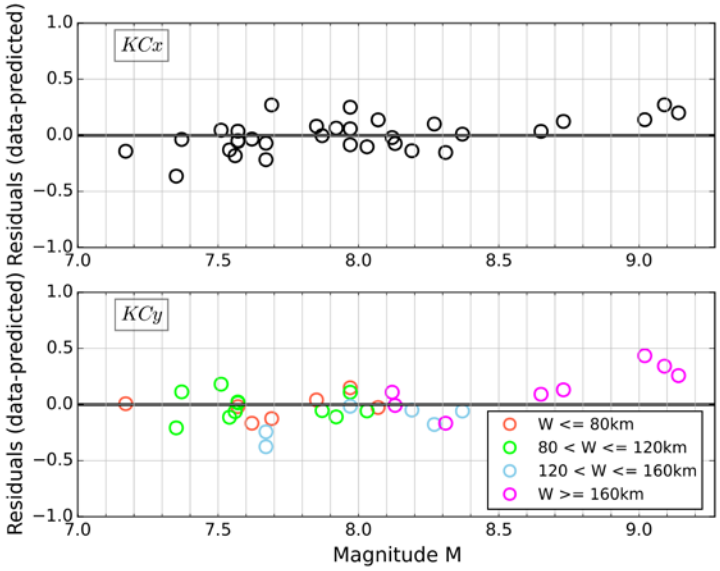

Figure 14. Residual distribution against magnitude (M) for c_x and c_y. The colored symbols in the bottom panel correspond to different fault width bins.

CONCLUSIONS

We compiled an updated database of interface earthquakes that occurred worldwide in the major subduction zones with moment magnitudes ranging from **M** 6.75 to **M** 9.17. We evaluated all available rupture models for each earthquake and selected the ones that were based on the largest number of strong motion or teleseismic data. In order to estimate the various source parameters we characterized the asperities for the original slip models based on a well-established methodology (Somerville et al., 1999).

We studied the scaling with seismic moment of rupture width, rupture area, total asperity area and of the average and maximum slip. In all cases the standard deviations are comparable if not smaller than the values estimated by Murotani et al. (2008; 2013). A factor that might have contributed to the smaller standard deviations is that we did not use more than one model of the same earthquake in the regression analysis. In cases where we had multiple source models for a single earthquake, we used judgment to select the most representative one based on various criteria such as the number and type of data used in deriving the model.

Despite the larger number of available data including the ones from the latest mega-thrust earthquakes, there are still few data to constrain the behavior of the scaling relations at high magnitudes (**M**>8.6). This limitation is prominent in the study of fault width scaling, for which several researchers suggest saturation of width (i.e. the down-dip rupture width stops growing beyond a certain magnitude resulting in constant width). In this study there were only three data points available at very large magnitudes. This high level of uncertainty makes it difficult to resolve the presence of width saturation. However, we consider that width saturation at a median width of 200 km is most likely present, but may vary from one subduction zone to another.

The differences in data fit between the unconstrained models and those that are constrained to be self-similar are not large and are not statistically significant. Therefore, we prefer to retain the simplicity of using the self-similar relations (Table 3) as found in some of the previous studies (Murotani et al., 2013; 2008, Somerville et al., 2002).

The comparison of the available scaling models of rupture area for both self-similar and non-self-similar functional forms presented in Figure 6 shows that there are still large differences between the models of the various authors. The results from our regression analysis of a large data set suggest that the Strasser et al., 2010, Blaser et al, 2010 and Papazachos et al., 2004 models are not consistent with the moment-area relation obtained from the data in Figure 6. Similarly, the Papazachos et al., 2004 model is not consistent with the moment- average displacement relation obtained from the data in Figure 7.

The differences in rupture areas between subduction and crustal earthquakes were originally identified by Somerville et al. (1999) and later by several other studies (e.g. Strasser et al., 2010; Murotani et al., 2008; 2013, Papazachos et al., 2004). Somerville et al. (1999) reported that on average, subduction earthquakes have rupture areas that are two or more times larger than those of crustal

earthquakes having the same seismic moment. In order to test this assumption with our dataset, we compared the scaling coefficients of Table 3 with the corresponding ones reported in Somerville et al. (1999) for crustal earthquakes. The results presented in Table 7 show that on average the rupture areas of subduction earthquakes are ~1.7 times larger and the average slip is ~0.4 times as large as those of crustal earthquakes having the same seismic moment.

Table 7. Comparison of parameters of scaling models of subduction and crustal earthquakes.

Parameter	Subduction	Crustal	Ratio
Rupture Area	1.77E-10	1.04E-10	1.70
Average Slip	1.23E-07	3.36E-07	0.37
Combined Area of Asperities	4.16E-11	2.32E-11	1.79
Fraction of fault covered by asperities	0.24	0.22	1.09

For the rupture area, the mean values computed in this study are very similar (within $\pm$1 standard deviation) of those reported in Murotani et al. (2008; 2013) (Figure 6, dashed green and red lines, respectively). The comparison of the present study results with those of Somerville et al. (2002) (light blue line) indicates smaller areas for the same seismic moment in the new relationships. For the average slip, the mean values computed in this study are similar to but lower than those estimated in Murotani et al. (2008; 2013) and higher than those in Somerville et al. (2002) (Figure 7). Figure 8 shows that the present study results estimate larger combined asperity areas for the same seismic moment than those in Murotani et al. (2008; 2013) and lower than in Somerville et al. (2002).

We also characterized the slip functions using wavenumber spectral models of the slip distribution. We resampled and zero padded the models in order to produce even sampling. The fitting of the 2D Butterworth filter function to estimate the corner wavenumbers for each direction involved a non-linear regression procedure solving the damped least squares equations using the Levenberg-Marquardt algorithm. The corner wavenumbers follow a self-similar scaling law with moment magnitude, as can be seen in Figure 13. The linear fit to the data does not exhibit any significant trends based on the residual analysis presented in Figure 14, except for magnitudes larger than 9. The along strike coefficient, c_x, has a very similar value compared to the one obtained in crustal earthquakes in Somerville et al. (1999), while the down-dip coefficient, c_y, has a lower value. Hence, for a given magnitude, subduction earthquake slip models exhibit heterogeneity in slip that is similar along strike but greater down-dip compared with crustal earthquakes.

REFERENCES

Ammon, C. J., J. Chen, H.-K. Thio, D. Robinson, S. Ni, V. Hjorleifsdottir, H. Kanamori, T. Lay, S. Das, D. Helmberger, G. Ichinose, J. Polet, and D. Wald. (2005). Rupture process of the great 2004 Sumatra-Andaman earthquake, *Science*, 308, 1133-1139.

Blaser, L., F. Krüger, M. Ohrnberger, and F. Scherbaum (2010). Scaling relations of earthquake source parameter estimates with special focus on subduction environment, *Bull. Seis. Soc. Am.*, 100, 2914–2926, doi:10.1785/0120100111.

Fujii, Y., and K. Satake (2013). Slip distribution and seismic moment of the 2010 and 1960 Chilean earthquakes inferred from tsunami waveforms and coastal geodetic data, *Pure Appl. Geophys.*, 170, 1493–1509.

Fukuyama, E. and K. Irikura (1986). Rupture process of the 1983 Japan Sea (Akita-Oki) earthquake using a waveform inversion method, *Bull. Seis. Soc. Am.*, 76, 1623–1640.

Hayes G. (NEIC, New Zealand 2009). Preliminary Result of the July 15, 2009 Mw 7.6 Fiordland Earthquake, http://earthquake.usgs.gov/earthquakes/eqinthenews/2009/us2009jcap/finite_fault.php.

Hayes G. (NEIC, Papua 2009). Preliminary Result of the Jan 3, 2009 Mw 7.6 Papua Earthquake, http://earthquake.usgs.gov/earthquakes/eqinthenews/2009/us2009bjbn/finite_fault.php.

Hayes G. (NEIC,Samoa 2009). Preliminary Result of the Sep 29, 2009 Mw 8.0 Samoa Earthquake, http://earthquake.usgs.gov/earthquakes/eqinthenews/2009/us2009mdbi/finite_fault.php.

Hayes G. (USGS, Philippines 2012). Preliminary Result of the Aug 31, 2012 Mw 7.6 earthquake east of Sulangan,Philippines,http://earthquake.usgs.gov/earthquakes/eqinthenews/2012/usc000cc5m/finite_fault.php.

Hayes G. (NEIC,Costa Rica 2012). Preliminary Result of the Sep 5, 2012 Mw 7.6 Costa Rica Earthquake, http://earthquake.usgs.gov/earthquakes/eqinthenews/2012/usc000cfsd/finite_fault.php.

Ichinose, G. A., H. K. Thio, P. G. Somerville, T. Sato, and T. Ishii (2003). Rupture process of the 1944 Tonankai earthquake (*M*s 8.1) from the inversion of teleseismic and regional seismograms, *J. Geophys. Res.*, 108, 2497, doi:10.1029/2003JB002393.

Ichinose, G., P. Somerville, H.-K. Thio, R. Graves, and D. O'Connell (2007). Rupture process of the 1964 Prince William Sound, Alaska, earthquake from the combined inversion of seismic, tsunami, and geodetic data, *J. Geophys. Res.*, 112, doi 10.1029/2006JB004728.

Ji C. and Y. Zeng (Peru 2007). Preliminary Result of the Aug 15, 2007 Mw 8.0 Coast of Central Peru Earthquake,http://earthquake.usgs.gov/earthquakes/eqinthenews/2007/us2007gbcv/finite_fault.php.

Ji C. and Y. Zeng (Sumatra 2005). Preliminary Result of the Sep 12, 2007 Mw 7.9 Kepulauan Earthquake, http://earthquake.usgs.gov/earthquakes/eqinthenews/2007/us2007hec6/finite_fault.php.

Ji, C. (UCSB, Benkulu 2007). Rupture Process of the Sep 12, 2007 Mw 8.4 Sumatra Earthquake: Phase II, http://www.geol.ucsb.edu/faculty/ji/big_earthquakes/2007/09/sumatra_seismic.html.

Ji, C. (UCSB,Kuril 2006). Rupture process of the 2006 Nov 15 Magnitude 8.3 - KURIL Island Earthquake(Revised),http://earthquake.usgs.gov/earthquakes/eqinthenews/2006/usvcam/finite_fault.php.

Ji, C. (UCSB, Solomon Islands 2007). Rupture process of the 2007 April 1, Magnitude 8.1, Solomon Islands Earthquake,http://earthquake.usgs.gov/earthquakes/eqinthenews/2007/us2007aqbk/finite_fault.php.

Johnson, J. M., and K. Satake (1999). Asperity distribution of the 1952 great Kamchatka earthquake and its relation to future earthquake potential in Kamchatka, *Pure Appl. Geophys.*, 154, 541–553.

Johnson, J.M., Y. Tanioka, L. J. Ruff, K. Satake,H. Kanamori, and L. R. Sykes (1994). The 1957 great Aleutian earthquake, *Pure Appl. Geophys.*, 142, 3–28.

Levenberg K., (1944). A Method for the Solution of Certain Non-Linear Problems in Least Squares, Quarterly of Applied Mathematics 2, 164–168.

Lorito, S., F. Romano, S. Atzori, X. Tong, A. Avallone, J. McCloskey, M. Cocco, E. Boschi, and A. Piatanesi (2011). Limited overlap between the seismic gap and coseismic slip of the great 2010 Chile earthquake, *Nature Geoscience*, 4, 173–177, doi:10.1038/ngeo1073.

Marquardt D., (1963). An Algorithm for Least-Squares Estimation of Nonlinear Parameters. SIAM Journal on Applied Mathematics 11, 431–441. doi:10.1137/0111030

Mendoza, C. and E. Fukuyama (1996). The July 12, 1993, Hokkaido Nansei-Oki, Japan, earthquake: Coseismic slip pattern from strong-motion and teleseismic recordings, *J. Geophys. Res.*, 101, 791–801.

Mendoza, C. and S. Hartzell (1989). Slip distribution of the 19 September 1985 Michoacan, Mexico, earthquake: near-source and teleseismic constraints, *Bull. Seis. Soc. Am*., 79, 655- 669.

Mendoza, C., and S. Hartzell. (1999). Fault-slip distribution of the 1995 Colima-Jalisco, Mexico, earthquake. *Bull. Seis. Soc. Am*, 89, 1338-1344.

Mendoza, C., S. Hartzell and T. Monfret, (1994). Wide-band analysis of the 3 March 1985 central Chile earthquake: overall source process and rupture history, *Bull. Seis. Soc. Am*., 84, 269-283.

Murotani, S., H. Miyake, and K. Koketsu (2008). Scaling of characterized slip models for plate-boundary earthquakes, *Earth Planets Space*, 60, 987–991.

Murotani, S., K. Satake and Y. Fujii (2013). Scaling relations of seismic moment, rupture area, average slip, and asperity size for M~9 subduction-zone earthquakes, *Geoph. Res. Lett.*, 40, 1-5.

Nagai, R., M. Kikuchi, and Y. Yamanaka (2001). Comparative study on the source processes of recurrent large *earthquakes* in Sanriku-oki region: the 1968 Tokachi-oki earthquake and the 1994 Sanriku-oki earthquake, *Zisin*, 54, 267–280 (in Japanese with English abstract).

Papazachos, B.C., E.M. Scordilis, D.G. Panagiotopoulos, C.B. Papazachos and G.F. Karakaisis (2004). Global relations between seismic fault parameters and moment magnitudes of earthquakes, *Bulletin of the Geological Society of Greece*, 36, 1482-1489.

Satake, K. (1993). Depth distribution of coseismic slip along the Nankai trough, Japan, from joint inversion of *geodetic* and tsunami data, *J. Geophys. Res.*, 98, 4553–4565.

Shao G. and C. Ji (UCSB, Honshu 2005). Preliminary Result of the Aug 16, 2005 Mw 7.19 Honshu Earthquake, http://www.geol.ucsb.edu/faculty/ji/big_earthquakes/2005/08/smooth/honshu.html.

Shao G. and C. Ji (UCSB, Masset 2012). Preliminary Result of the Oct 28, 2012 Mw 7.72 Canada Earthquake, http://www.geol.ucsb.edu/faculty/ji/big_earthquakes/2012/10/canada.html.

Shao G. and C. Ji (UCSB, Sumatra 2005). Preliminary Result of the Mar 28, 2005 Mw 8.68 nais Earthquake, http://www.geol.ucsb.edu/faculty/ji/big_earthquakes/2005/03/smooth/nias.html.

Sladen A. (Caltech, Tocopilla 2007). Preliminary Result 11/14/2007 (Mw 7.7), Tocopilla Earthquake, Chile. Source Models of Large Earthquakes. http://www.tectonics.caltech.edu/slip_history/2007_tocopilla/tocopilla.html.

Sladen A. (Caltech, Vanuatu 2009). Preliminary Result 10/07/2009 (Mw 7.6), Vanuatu. Source Models of Large Earthquakes. http://www.tectonics.caltech.edu/slip_history/2009_vanuatu/index.html.

Somerville P.G., H.K. Thio, G. Ichinose, N. Collins, A. Pitarka, and R. Graves (2003). Earthquake source and ground motion characteristics of the June 23, 2001 Mw 8.4 Arequipa, Peru, earthquake, *Seis. Res. Lett.* 74, 223.

Somerville P.G., K. Irikura, R. Graves, S. Sawada, D. Wald, N. Abrahamson, Y. Iwasaki, T. Kagawa, N. Smith, and A. Kowada, (1999). Characterizing crustal earthquake slip models for the prediction of strong ground motion, *Seis. Res. Lett.* 70, 59–80.

Somerville P.G., T. Sato, T. Ishii, N.F. Collins, K. Dan and H. Fujiwara (2002). Characterizing heterogeneous slip models for the large subduction earthquakes for strong ground motion prediction. *Proc. 11th Japan Earthquake Engineering Symposium*, 163-166 (in Japanese with English abstract).

Spence, W., C. Mendoza, E. R. Engdahl, G. L. Choy, and E. Norabuena (1999). Seismic subduction of the Nazca Ridge as shown by the 1996-97 Peru earthquakes, *Pure and Applied Geophysics*, 154, 753-776.

Strasser F.O., M.C. Arango, and J.J. Bommer (2010). Scaling of the source dimensions of interface and intraslab subduction-zone earthquakes with moment magnitude, *Seis. Res. Lett.* 81, 941–950.

Tajima R., Y. Matsumoto, H. Si and K. Irikura, (2013). Comparative Study on Scaling Relations of Source Parameters for Great Earthquakes in Inland Crusts and on Subducting Plate Boundaries, *Zisin* 66, 31-45. Doi:10.4294/zisin.66.31 (in Japanese with English abstract).

Wald, D. J. and P. G. Somerville (1995). Variable-slip rupture model of the great 1923 Kanto, Japan, earthquake: Geodetic and body-waveform analysis, *Bull. Seis. Soc. Am.*, **85**, 159–177.

Wei S. (Caltech, Oaxaca 2012). March/20/2012 (Mw 7.4), OAXACA, Mexico. Source Models of Large Earthquakes. http://www.tectonics.caltech.edu/slip_history/2012_Mexico/index.html.

Yagi, Y. (2004). Source rupture process of the 2003 Tokachi-oki earthquake determined by joint inversion of teleseismic body wave and ground motion data, *Earth Planets Space*, 56, 311–316.

Yagi, Y., M. Kikuchi, S. Yoshida, and Y. Yamanaka (1998). Source process of the Hyuga-nada earthquake of April 1, 1968 (*M*JMA 7.5), and its relationship to the subsequent seismicity, *Zisin*, 51, 139–148 (in Japanese with English abstract).

Yagi, Y., T. Mikurno, J. Pacheco, and G. Reyes (2004). Source rupture process of the Tecoman, Colima, Mexico earthquake of 22 January 2003, determined by joint inversion of teleseismic body-wave and near-source data, *Bull. Seis. Soc. Am*, 94, 1795-1807.

Yagi, Y.,M. Kikuchi, S. Yoshida, and T. Sagiya (1999). Comparison of the coseismic rupture with the aftershock distribution in the Hyuga-nada earthquakes of 1996, *Geophys. Res. Lett.*, 26, 3161–3164.

Yokota Y., K. Koketsu, Y. Fujii, K. Satake, S. Sakai, M. Shinohara, and T. Kanazawa (2011). Joint inversion of strong motion, teleseismic, geodetic, and tsunami datasets for the rupture process of the 2011 Tohoku earthquake, *Geophys. Res. Lett.*, 38, doi:10.1029/2011GL050098.